

more general Moore–Penrose method, and is specific to the particular problem discussed here. This is because it relies on certain properties of a tree graph, as can be seen from what follows.

\mathbf{B}_T is a matrix in which each column contains one element of value 1, one -1 , and the rest zero. The corresponding row of its inverse has only values $\pm \frac{1}{2}$, the sign depending on whether that vertex lies in the same component of the graph as the positive or negative end of the corresponding edge used as cut. Table 1 gives the $K^{2,3}$ case. For programming purposes the components are best determined from a matrix of distances within the spanning tree T , for then each vertex takes the sign of the nearer end of the edge which is cut. The distance matrix is constructed by first forming the adjacency matrix of the tree, \mathbf{A}_T , using $\mathbf{A}_T = \mathbf{B}\mathbf{B}' - \mathbf{V}$ where \mathbf{V} is a diagonal matrix of the vertex degrees.

Then the zero elements A_{Tik} are found for which A_{Tij} and A_{Tjk} are both non-zero, and are filled in with the distance of the path ijk , namely $A_{Tij} + A_{Tjk}$. Repetition of this procedure will find all distances up

to and including 2, 4, 8 ... and so on, until the distance matrix is complete.

It is now possible to determine each element of \mathbf{B}_T^{-1} by comparing two elements of this distance matrix, which we may call \mathbf{P} . However, the programming may be made even simpler by noting

$$\mathbf{B}_T^{-1'} = -\frac{1}{2}\mathbf{P}\mathbf{B}_T.$$

References

- BOLLOBÁS, B. (1979). *Graph Theory*, pp. 38–40. New York: Springer-Verlag.
 BROWN, I. D. (1977). *Acta Cryst.* **B33**, 1305–1310.
 BROWN, I. D. (1981). *Structure and Bonding in Crystals*, Vol. 2, edited by M. O'KEEFE & A. NAVROTSKY, pp. 1–30. New York: Academic Press.
 BROWN, I. D. & SHANNON, R. D. (1973). *Acta Cryst.* **A29**, 266–282.
 DE VREIS, R. & MIJLHOFF, F. C. (1969). *Acta Cryst.* **B25**, 1696–1699.
 EVANS, H. T. JR (1960). *Z. Kristallogr.* **114**, 257–277.
 MACKAY, A. L. & FINNEY, J. L. (1973). *J. Appl. Cryst.* **6**, 284–289.
 MEIER, W. M. & VILLIGER, H. (1969). *Z. Kristallogr.* **129**, 411–423.
 PAULING, L. (1929). *J. Am. Chem. Soc.* **51**, 1010–1026.

Acta Cryst. (1990). **B46**, 292–301

On the Crystal Structure of Staurolite. The X-ray Crystal Structure of Staurolite from the Pyrenees and Brittany

BY KENNY STÅHL

Inorganic Chemistry 2, University of Lund, PO Box 124, S-221 00 Lund, Sweden

AND JEAN-PIERRE LEGROS

Laboratoire de Chimie de Coordination, CNRS, 205 route de Narbonne, F-31077 Toulouse CEDEX, France

(Received 9 October 1989; accepted 8 December 1989)

Abstract

The crystal structures of two natural crystals of staurolite, from Heas, the Pyrenees (*H*), and Scaer, Brittany (*S*), France, have been refined from X-ray Mo $K\alpha$ data at 293 K. Monoclinic, $C2/m$, $Z = 1$. (*H*): $\text{Fe}_{3.59}\text{Ti}_{0.09}\text{Mn}_{0.01}\text{Zn}_{0.01}\text{Mg}_{0.83}\text{Al}_{17.90}\text{Si}_{7.50}\text{O}_{45}(\text{OH})_3$, $M_r = 1690.8$, $D_x = 3.79 \text{ g cm}^{-3}$, $\mu = 28.01 \text{ cm}^{-1}$, $a = 7.8700$ (9), $b = 16.6228$ (18), $c = 5.6613$ (4) Å, $\beta = 90.124$ (5)°, $V = 740.6$ (2) Å³, $R(F) = 0.018$ for 2494 unique reflections. (*S*): $\text{Fe}_{3.38}\text{Ti}_{0.11}\text{Mn}_{0.06}\text{Zn}_{0.47}\text{Mg}_{0.75}\text{Al}_{17.81}\text{Si}_{7.66}\text{O}_{45}(\text{OH})_3$, $M_r = 1684.9$, $D_x = 3.777 \text{ g cm}^{-3}$, $\mu = 27.52 \text{ cm}^{-1}$, $a = 7.8713$ (2), $b = 16.6235$ (7), $c = 5.6608$ (2) Å, $\beta = 90.016$ (2)°, $V = 740.71$ (8) Å³, $R(F) = 0.026$ for 2997 unique reflections. It is demonstrated that the crystal structure of staurolite can be derived from that of spinel through crystallographic shear. The geometric

differences between the (*H*) and (*S*) varieties and previously studied staurolites are confined to the partially occupied cation sites. The disorder in the tetrahedral Fe site can be effectively modelled using third- and fourth-order coefficients of a Gram–Charlier expansion of the Fe temperature factor or by a threefold-split Fe(*A/B/C*) site. Model calculations demonstrated that neither the difference electron density ($\Delta\rho$) peak separation, nor the $\Delta\rho$ peak heights, are directly interpretable, while the increase in temperature-factor coefficients owing to disorder is reliably related to the site splitting. The separation between the Fe(*A/B/C*) positions is estimated to be 0.25 Å. The large variation between previously reported Fe-site $\Delta\rho$ peak separations can be related to different experimental resolutions. The present study suggests that the Fe-site splitting is in the range 0.20–0.25 Å for all staurolites.

Introduction

The crystal structure of staurolite has been subject to numerous diffraction studies since it was first suggested by Náray-Szabó (1929) using the orthorhombic space group $Ccmm$. Optical and X-ray film measurements by Hurst, Donnay & Donnay (1956) demonstrated that the true symmetry is monoclinic and X-ray structure redeterminations by Náray-Szabó & Sasvari (1958) and Smith (1968) established the space group $C2/m$ and the principal site occupancies. Through neutron diffraction studies the hydrogen positions were successively determined by Takéuchi, Aikawa & Yamamoto (1972), Tagai & Joswig (1985) and Ståhl, Kvik & Smith (1985, 1988). In the latter investigation a second set of hydrogen positions with a total occupancy of $\sim 25\%$ was found. These hydrogen sites [H(2A) and H(2B), *cf.* Fig. 3] are ~ 1.4 Å from the tetrahedral Fe site, and they cannot be simultaneously occupied. This led to a reinterpretation of the Fe-site composition: to achieve the scattering power observed by X-ray and neutron diffraction for a partially occupied Fe site, almost all Fe present has to be located in this site. Also the splitting of the Fe Mössbauer spectrum and its temperature dependence can be straightforwardly interpreted assuming almost all Fe in a disordered tetrahedral site (Dowty, 1972). Structure determinations of Zn-rich (Hanisch, 1966) and Co-rich (Bringhurst & Griffen, 1986) staurolites, as well as recent progress in the determination of H (Lonker, 1983; Holdaway, Dutrow & Shore, 1986) and Li (Dutrow, Holdaway & Hinton, 1986), have also added significantly to the understanding of staurolite crystal chemistry.

Despite many structure determinations, several uncertainties remain concerning the crystal chemistry of staurolite, *e.g.* the effects of compositional variations and the nature and extent of the disorder of the tetrahedral Fe position. The present paper will discuss the structural relationships and properties (especially the Fe-site disorder) of staurolite, invoking the results from two high-precision X-ray structure refinements using natural single crystals from different localities: Heas, the Pyrenees [the locality is described by Moreau (1975)] and Scaer, Brittany [the locality is described by Chauris & Le Bail (1968)]. The two localities are hereafter denoted (*H*) and (*S*), respectively.

Experimental

Electron microprobe analyses

The analyses were carried out on a Camebax SX50 at Université Paul-Sabatier, Toulouse, using 15 kV and 20 nA. Standards used were for Fe: Fe_2O_3 , Si:

SiO_2 , Al: Al_2O_3 , Ti: TiO_2 , Mn: graffonite, Zn: ZnS, and Mg: MgO. The results were normalized to 48 O and, following Holdaway *et al.* (1986), to 3 H. All Fe was assumed to be Fe^{II} . Each crystal was measured at four different positions. The analyses gave for the crystal from Heas, the Pyrenees (*H*), a composition of $Fe_{3.59}Ti_{0.09}Mn_{0.01}Zn_{0.01}Mg_{0.83}Al_{17.90}Si_{7.50}O_{45}(OH)_3$ and for the crystal from Scaer, Brittany (*S*), $Fe_{3.38}Ti_{0.11}Mn_{0.06}Zn_{0.04}Mg_{0.75}Al_{17.81}Si_{7.66}O_{45}(OH)_3$.

X-ray diffraction data

Both data sets were collected at 293 K using graphite-monochromatized $Mo K\alpha$ radiation, $\omega/2\theta$ scans, constant detector opening, in a hemisphere with $2 \leq \theta \leq 45^\circ$ and indices satisfying $h+k$ even.

(*H*). The crystal was bounded approximately by $\{100\}$, $\{010\}$ and $\{001\}$, $0.16 \times 0.24 \times 0.26$ mm. Unit-cell dimensions were determined from least-squares refinements of 75 2θ values with $23 \leq 2\theta \leq 60^\circ$. The data were collected on an Enraf-Nonius CAD-4 diffractometer, where the scan speeds were determined from pre-scans, requiring $I > 2\sigma(I)$ for a reflection to be considered observed and for a final scan to be performed, and a maximum time of 180 s. The data collection was limited by $-15 \leq h \leq 0$, $-33 \leq k \leq 33$ and $-11 \leq l \leq 11$. Two standard reflections measured every 6000 s of X-ray exposure showed no significant variation.

(*S*). The crystal was bounded approximately by $\{100\}$, $\{1\bar{1}0\}$ and $\{001\}$, $0.18 \times 0.22 \times 0.16$ mm. Unit-cell dimensions were determined from least-squares refinement of 69 2θ values with $34 \leq 2\theta \leq 61^\circ$. The data were collected on a Huber diffractometer. The scan speed was 2° min^{-1} with an additional scan at $0.4^\circ \text{ min}^{-1}$ for reflections with $3 < I/\sigma(I) < 40$. All reflections having $I > 0$ were included in the refinements. The data collection was limited by $-15 \leq h \leq 15$, $0 \leq k \leq 33$ and $-11 \leq l \leq 11$. The two standard reflections measured every 6000 s of X-ray exposure time showed a 10% linear decrease owing to X-ray tube decay and the intensities were corrected accordingly.

Both data sets were corrected for the Lorentz effect and polarization. Absorption corrections were made numerically through Gaussian integration over an $8 \times 8 \times 8$ grid. Additional information concerning the data collection, reduction and structure refinements is given in Table 1.

Structure refinements

The full-matrix least-squares refinements minimized $\sum w(F_o^2 - F_c^2)^2$, where $w = [\sigma^2(F_o^2) + (c_1 F_o^2)^2 + c_2^2]^{-1}$ with $\sigma(F_o^2)$ from counting statistics and c_1 and c_2 adjusted to give constant $\langle w\Delta F^2 \rangle$ in different F_o^2 and $\sin\theta$ intervals. As recommended by Schwarzenbach

Table 1. *Crystal data, data collection and least-squares refinement details for staurolite, refinement model (II), space group C2/m*

| | Heas | Scaer |
|--------------------------------|-------------------------|-------------------------|
| a (Å) | 7.8700 (9) | 7.8713 (2) |
| b (Å) | 16.6228 (18) | 16.6235 (7) |
| c (Å) | 5.6613 (4) | 5.6608 (2) |
| β (°) | 90.124 (5) | 90.016 (2) |
| V (Å ³) | 740.6 (2) | 740.71 (8) |
| M_r | 1690.9 | 1684.9 |
| D_r (g cm ⁻³) | 3.791 | 3.777 |
| μ (cm ⁻¹) | 28.01 | 27.52 |
| Range of transmission factors | 0.51–0.63 | 0.63–0.73 |
| Scan widths (°) | 0.9 + 0.35 tan θ | 1.0 + 0.50 tan θ |
| Isotropic extinction parameter | 0.15 (1) $\times 10^4$ | 0.35 (2) $\times 10^4$ |
| No. of reflections collected | 4750 | 6318 |
| unique in final LS cycle | 2506 | 2997 |
| No. of parameters refined | 116 | 115 |
| R_{int} | 0.016 | 0.018 |
| $R(\langle F \rangle)$ | 0.018 | 0.026 |
| $R(F)$ | 0.020 | 0.031 |
| $R(F^2)$ | 0.029 | 0.034 |
| $wR(F^2)$ | 0.049 | 0.052 |
| S | 1.07 | 1.32 |
| Weighting constants c_1 | 0.035 | 0.030 |
| c_2 | 9.95 | 9.50 |

et al. (1989), the unaveraged data sets were used in refinements. $R(\langle F \rangle)$ in the following refers to the conventional reliability factor calculated from unique averaged reflections. The refinements were started with parameters from Smith (1968). In the first model 108 parameters were refined, including positional parameters, anisotropic temperature-factor coefficients for all atoms except those in the $U(A)$ and $U(B)$ sites, occupancy factors for Fe, Al(3A), Al(3B), $U(A)$ and $U(B)$, one scale factor and one isotropic extinction parameter [type 1, Lorentzian mosaicity (Becker & Coppens, 1974)]. The occupancy factors of Si, Al(1A), Al(1B) and Al(2) were initially refined, but did not differ significantly from unity and were kept constant in the final cycles. The U sites are occupied by various atoms (Smith, 1968); Fe was assumed in the refinements. This model (I) refined to $R(\langle F \rangle) = 0.026$ (H) and 0.036 (S). Difference electron density ($\Delta\rho$) maps showed high residual peaks about the Fe position (Fig. 1). Introducing γ and δ parameters of the Gram–Charlier expansion of the Fe temperature factor resulted in a dramatic improvement, and with this model (II) the refinements converged to $R(\langle F \rangle) = 0.018$ (H) and 0.026 (B). Only anharmonic components differing from zero by more than two e.s.d.'s were refined in the final cycles. In refinement model (III), the Fe disorder was modelled with a threefold-split Fe site. The split positions were placed in the corners of a fixed 0.25 Å equilateral triangle (see *Discussion*). The Fe parameters refined initially included the x coordinate of the triangle and finally three independent occupancy factors and anisotropic temperature-factor coefficients, independent on Fe(C) and coupled between Fe(A) and Fe(B). Model (III) refined to $R(\langle F \rangle) = 0.019$ (H) and 0.027 (S). Less-constrained refinements were unstable owing to

strong correlations. The refinements were considered to have converged when the largest (parameter shift)/(parameter e.s.d.) < 0.03 . The highest $\Delta\rho$ peaks from models (II) and (III) were 0.8 e Å⁻³ in the vicinity of O(1A) and O(1B) for both (H) and (S). The final $\Delta\rho$ maps in the vicinity of the Fe site are shown in Fig. 1. The refined non-Fe parameters agreed within one e.s.d. between models (II) and (III) and within three e.s.d.'s between models (I) and (II). A comparison of Fe parameters from the different models is given in Table 2. The final atomic parameters given in Table 3 and the selection of distances and angles given in Table 4 all relate to refinement model (II) in order to have consistent parameter sets.*

In the (H) structure the β angle of the unit cell as well as the presence of some weak $0kl$ reflections violates the orthorhombic space group $Ccmm$. In the (S) structure the deviation from 90° in β angle is small and the reflection data obey the extinction rules for space group $Ccmm$. Averaging reflections after data reduction according to monoclinic symmetry gave $R_{int} = 0.016$ (H) and 0.018 (S). Further averaging according to orthorhombic symmetry resulted in $R_{int} = 0.047$ (H) and 0.013 (S). Refinements of model (I) in space group $Ccmm$ resulted in $R(\langle F \rangle)$ values of 0.046 (H) and 0.038 (S), again in favour of monoclinic (H) and orthorhombic (S). However, as the refinement in $Ccmm$ neither significantly changed the (S) parameters, nor improved the e.s.d.'s the (S) structure is here presented as monoclinic in order to simplify comparisons with the (H) structure and previously studied staurolites.

Scattering factors for neutral atoms and anomalous-scattering corrections were taken from *International Tables for X-ray Crystallography* (1974). The crystallographic computer programs have been described by Lundgren (1983).

Discussion

Structural relationships

The staurolite structure is commonly described as being built from alternating layers of cyanite, Al₂SiO₅, and \sim Fe₂Al_{0.7}O₂(OH)₂ (Náray-Szabó, 1929). However, the complicated way in which the structure is built up from these layers (Griffen, Gosney & Phillips, 1982) makes the model very difficult to visualize. Fig. 2 demonstrates how the

* Complete lists of coordinates and anisotropic temperature-factor coefficients from models (I), (II) and (III), together with bond angles, and observed and calculated structure factors from model (II) have been deposited with the British Library Document Supply Centre as Supplementary Publication No. SUP 52526 (86 pp.). Copies may be obtained through The Technical Editor, International Union of Crystallography, 5 Abbey Square, Chester CH1 2HU, England.

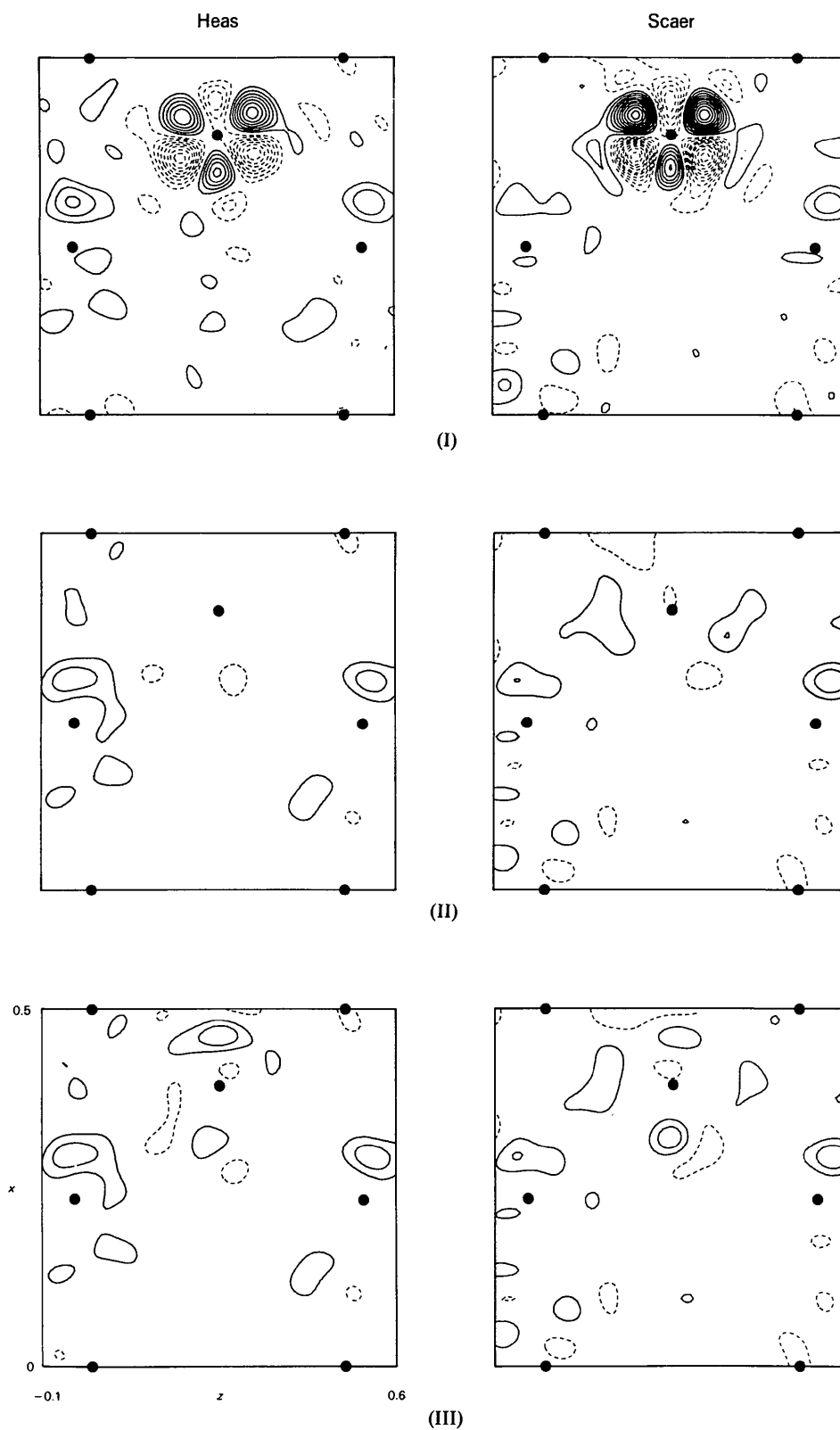


Fig. 1. $\Delta\rho$ maps in the $y = 0$ plane of staurolite using only harmonic (I) and including anharmonic (II) temperature-factor coefficients and finally a split-Fe position (III). The atomic positions are explained in Fig. 3. Levels at $0.3 \text{ e } \text{\AA}^{-3}$, negative levels broken and zero level omitted.

Table 2. Comparison of refinements using harmonic (I) and anharmonic (II) temperature-factor expressions, or split (III) Fe sites in staurolite

| | (I), (II)/(III) | Heas | | | Scaer | | |
|---|-----------------|---------------|---------------|--------------|---------------|---------------|--|
| | (I) | (II) | (III) | (I) | (II) | (III) | |
| $x/(x)$ | 0.39260 (3) | 0.39279 (5) | 0.39264 | 0.39134 (3) | 0.39191 (5) | 0.39177 | |
| $z/(z)$ | 0.24833 (5) | 0.24889 (7) | 0.24855 | 0.24987 (5) | 0.24986 (4) | 0.24984 | |
| g/g_{sum} | 0.820 (1) | 0.817 (1) | 0.812 (2) | 0.863 (1) | 0.857 (1) | 0.855 (2) | |
| $B_{11}/B_{11}^{\text{iso}} (\text{Å}^2)$ | 0.01962 (10) | 0.01929 (10) | 0.00906 (11) | 0.01935 (11) | 0.01801 (19) | 0.00697 (12) | |
| $B_{22}/B_{22}^{\text{iso}} (\text{Å}^2)$ | 0.00571 (7) | 0.00574 (6) | 0.00472 (10) | 0.00567 (7) | 0.00568 (6) | 0.00467 (11) | |
| $B_{33}/B_{33}^{\text{iso}} (\text{Å}^2)$ | 0.02231 (11) | 0.02107 (19) | 0.01082 (21) | 0.02220 (11) | 0.02094 (20) | 0.01242 (24) | |
| $B_{12}/B_{12}^{\text{iso}} (\text{Å}^2)$ | -0.00022 (5) | -0.00004 (6) | 0.00012 (10) | 0.0004 (5) | 0.00006 (7) | -0.00025 (11) | |
| $\gamma_{111}/B_{11}^{\text{iso}}$ | — | -0.00048 (3) | 0.00611 (21) | — | -0.00030 (3) | 0.00505 (17) | |
| $\gamma_{333}/B_{33}^{\text{iso}}$ | — | 0.00090 (11) | 0.00832 (24) | — | — | 0.00736 (18) | |
| $\gamma_{122}/B_{22}^{\text{iso}}$ | — | -0.000040 (3) | 0.00780 (29) | — | -0.000033 (3) | 0.01028 (25) | |
| $\gamma_{112}/B_{11}^{\text{iso}}$ | — | 0.00028 (3) | -0.00008 (11) | — | — | 0.00014 (9) | |
| $\gamma_{133}/g^{\text{A}}$ | — | 0.00197 (4) | 0.312 (1) | — | 0.00221 (4) | 0.270 (1) | |
| $\delta_{1111}/g^{\text{B}}$ | — | — | 0.258 (1) | — | -0.00024 (4) | 0.264 (1) | |
| $\delta_{3333}/g^{\text{C}}$ | — | -0.00091 (2) | 0.242 (1) | — | -0.00092 (2) | 0.321 (1) | |
| δ_{1333} | — | 0.00016 (1) | — | — | 0.0002 (1) | — | |
| δ_{1133} | — | -0.00027 (3) | — | — | -0.00025 (3) | — | |
| n_{max} | 108 | 116 | 111 | 108 | 115 | 111 | |
| $R((F))$ | 0.0256 | 0.0182 | 0.0192 | 0.0370 | 0.0271 | 0.0274 | |
| S | 1.37 | 1.07 | 1.11 | 1.68 | 1.32 | 1.34 | |

Table 3. Final atomic fractional coordinates ($\times 10^5$), refined occupancy factors, g , and thermal parameters with e.s.d.'s for staurolite from Heas and Scaer

| | $B_{\text{iso}} = (4/3)\sum_i \sum_j B_{ij} a_i a_j$ | | | | |
|--------------|--|-----------|------------|-----------|-------------------------------|
| | x | y | z | g | $B_{\text{iso}} (\text{Å}^2)$ |
| Heas | | | | | |
| Fe | 39279 (5) | 0 | 24889 (7) | 0.817 (1) | 1.213 (6) |
| $U(A)$ | 50000 | 0 | 0 | 0.064 (1) | 0.94 (5) |
| $U(B)$ | 50000 | 0 | 50000 | 0.034 (1) | 1.04 (10) |
| Si | 13411 (2) | 16606 (1) | 24900 (3) | — | 0.335 (2) |
| Al(1A) | 50000 | 17526 (1) | 0 | — | 0.389 (4) |
| Al(1B) | 50000 | 17510 (1) | 50000 | — | 0.396 (4) |
| Al(2) | 26333 (2) | 41033 (1) | 25118 (3) | — | 0.466 (3) |
| Al(3A) | 0 | 0 | 0 | 0.588 (3) | 0.477 (10) |
| Al(3B) | 0 | 0 | 50000 | 0.406 (3) | 0.500 (15) |
| O(1A) | 23344 (8) | 0 | 96396 (11) | — | 0.703 (9) |
| O(1B) | 23521 (8) | 0 | 53395 (12) | — | 0.752 (9) |
| O(2A) | 25533 (5) | 16148 (2) | 1522 (7) | — | 0.462 (6) |
| O(2B) | 25470 (5) | 16122 (2) | 48422 (7) | — | 0.468 (6) |
| O(3) | 174 (5) | 8880 (2) | 24692 (8) | — | 0.683 (6) |
| O(4) | 2132 (5) | 24917 (2) | 24976 (7) | — | 0.475 (5) |
| O(5) | 52712 (5) | 10013 (2) | 24962 (7) | — | 0.472 (5) |
| Scaer | | | | | |
| Fe | 39191 (5) | 0 | 24986 (4) | 0.857 (1) | 1.175 (7) |
| $U(A)$ | 50000 | 0 | 0 | 0.030 (1) | 0.75 (11) |
| $U(B)$ | 50000 | 0 | 50000 | 0.029 (1) | 0.76 (11) |
| Si | 13409 (2) | 16603 (1) | 24992 (3) | — | 0.306 (2) |
| Al(1A) | 50000 | 17529 (2) | 0 | — | 0.360 (0) |
| Al(1B) | 50000 | 17528 (2) | 50000 | — | 0.357 (4) |
| Al(2) | 26303 (2) | 41048 (1) | 25009 (3) | — | 0.437 (3) |
| Al(3A) | 0 | 0 | 0 | 0.507 (3) | 0.432 (13) |
| Al(3B) | 0 | 0 | 50000 | 0.496 (3) | 0.464 (13) |
| O(1A) | 23445 (9) | 0 | 96478 (12) | — | 0.725 (9) |
| O(1B) | 23467 (9) | 0 | 53498 (12) | — | 0.735 (10) |
| O(2A) | 25512 (5) | 16130 (3) | 1548 (7) | — | 0.448 (6) |
| O(2B) | 25508 (5) | 16134 (3) | 48453 (7) | — | 0.446 (6) |
| O(3) | 174 (5) | 8876 (3) | 24979 (9) | — | 0.667 (6) |
| O(4) | 2143 (3) | 24913 (2) | 25002 (7) | — | 0.451 (5) |
| O(5) | 52680 (5) | 10028 (2) | 25001 (7) | — | 0.445 (6) |

complete staurolite structure (Fig. 2b) can be derived from the well known spinel structure (Fig. 2a) applying simple crystallographic shear (Andersson & Hyde, 1982). The arrows (Fig. 2a) indicate the shear planes at about $y = \frac{1}{4}$ and $\frac{3}{4}$ (coordinates referring to the staurolite unit cell). The shear planes extend throughout the single crystal. A translation, $z' = z + \frac{1}{2}$, of the section between the arrows will now generate the staurolite structure (Fig. 2b). The

Table 4. Selected bond distances (Å) in staurolite

Superscripts indicate number of symmetry-equivalent distances.

| | Heas | Scaer |
|----------------------------|------------|------------|
| Fe—O(1A) | 2.0411 (8) | 2.0341 (8) |
| Fe—O(1B) | 2.0374 (8) | 2.0338 (8) |
| Fe—O(5) ² | 1.9718 (5) | 1.9762 (5) |
| $U(A)$ —O(1A) ² | 2.1073 (7) | 2.0991 (7) |
| $U(A)$ —O(5) ⁴ | 2.1936 (4) | 2.1966 (4) |
| $U(B)$ —O(1B) ² | 2.0932 (7) | 2.0974 (7) |
| $U(B)$ —O(5) ⁴ | 2.1970 (4) | 2.1966 (4) |
| Si—O(2A) | 1.6349 (4) | 1.6354 (4) |
| Si—O(2B) | 1.6355 (4) | 1.6355 (4) |
| Si—O(3) | 1.6537 (4) | 1.6535 (5) |
| Si—O(4) | 1.6421 (4) | 1.6414 (4) |
| Al(1A)—O(2A) ² | 1.9412 (4) | 1.9430 (4) |
| Al(1A)—O(4) ² | 1.8986 (4) | 1.8997 (5) |
| Al(1A)—O(5) ² | 1.8975 (4) | 1.8975 (4) |
| Al(1B)—O(2B) ² | 1.9462 (4) | 1.9432 (4) |
| Al(1B)—O(4) ² | 1.9029 (4) | 1.8996 (5) |
| Al(1B)—O(5) ² | 1.8997 (4) | 1.8975 (4) |
| Al(2)—O(1A) | 1.9251 (5) | 1.9219 (5) |
| Al(2)—O(1B) | 1.9239 (5) | 1.9220 (5) |
| Al(2)—O(2A) | 1.9287 (4) | 1.9243 (5) |
| Al(2)—O(2B) | 1.9182 (4) | 1.9239 (5) |
| Al(2)—O(3) | 1.8765 (5) | 1.8785 (5) |
| Al(2)—O(5) | 1.8671 (5) | 1.8675 (4) |
| Al(3A)—O(1A) ² | 1.8489 (6) | 1.8558 (7) |
| Al(3A)—O(3) ⁴ | 2.0330 (5) | 2.0434 (5) |
| Al(3B)—O(1B) ² | 1.8606 (7) | 1.8572 (7) |
| Al(3B)—O(3) ⁴ | 2.0572 (5) | 2.0451 (5) |

unhatched octahedra in Fig. 2(a) are occupied in spinel, but are lost in the shear operation.

In staurolite the tetrahedral positions on each side of the shear planes are all occupied by Si^{4+} , except for minor Al^{3+} substitution. The high formal valence on this tetrahedral cation assures a valence sum of two on O(4) and should be an inherent property of this structure type. The Al(2) octahedral pairs sharing an edge (Fig. 2b) show a typical increased Al(2)—Al(2) separation and a shortening of the common edge, O(1A)—O(1B). The resulting enlarged tetrahedra between the Al(2) octahedral pairs (the Fe site) are another inherent property of the staurolite structure type. Also the distortion of the $U(A/B)$ octahedra can be explained by an increased Al(2)—Al(2) distance (elongation in the b

direction) and a shortened O(1A)—O(1B) edge (the tilt with respect to **a**).

The similarity between the Fe environment in sections of staurolite and the spinel hercynite, Al_2FeO_4 , was recognized by Hollister (1970), and it is interesting to note that a spinel–hercynite intermediate given as $\sim\text{Al}_2(\text{Fe}_{0.8}\text{Mg}_{0.2})\text{O}_4$ has been identified in the Heas material (Moreau, 1975).

Domain description

Based on crystal-chemical reasoning it has been suggested that staurolite is an ensemble of three pairs of structural domains 1A, 1B, 2A, 2B, 3A and 3B (Ståhl *et al.*, 1988). Structural domains 1A and 1B have fully occupied Fe sites and empty U sites, fully occupied Al(3A) and H(1A) in subdomain A, and Al(3B) and H(1B) sites in subdomain B (*cf.* Fig. 3).

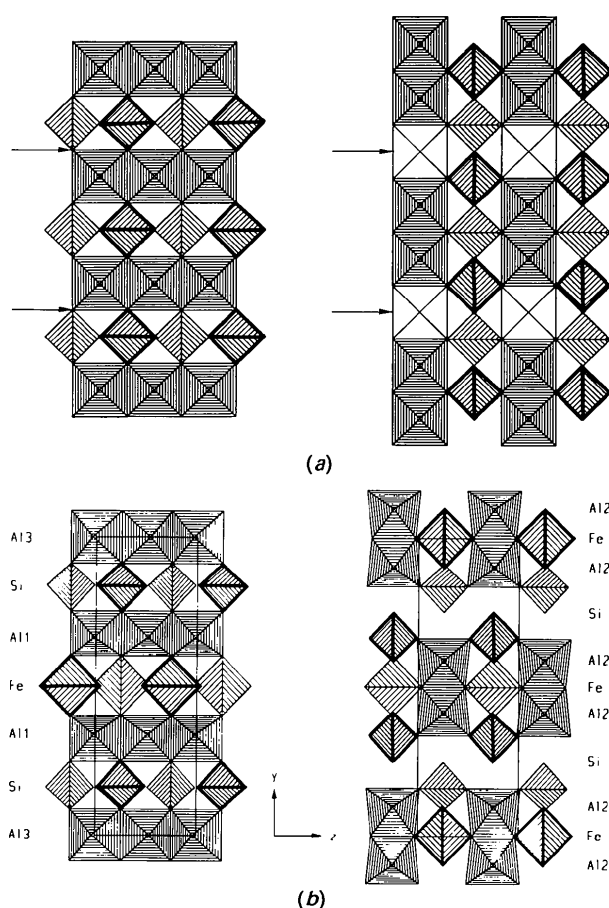


Fig. 2. (a) Projected sections of the spinel structure. Arrows indicate the shear planes. Unhatched octahedra (right) are occupied in spinel but lost in the shear operation ($z' = z + \frac{1}{2}$). (b) Projected *bc* sections of the staurolite structure. Mean octahedral levels are $x = 0$ (left) and 0.25 (right). Bold tetrahedral levels are $x = 0.125$ (left) and 0.375 (right), regular tetrahedra $x = -0.125$ (left) and 0.125 (right). The unit cell is indicated as a solid line.

Domains 2A and 2B have empty Fe sites, partially occupied U sites and one of the H(2) sites occupied. Structural domains 3A and 3B differ from 1A and 1B in that H(1A) and H(1B) are always empty. Fig. 2(b) thus corresponds to a superposition of structural domains 1A, 1B, 3A and 3B. Subdomains A and B are related by a $c/2$ translation. In the special case of equal amounts of A and B, staurolite will show orthorhombic symmetry (*Ccmm*). In the general case of unequal amounts of A and B, the symmetry will be monoclinic (*C2/m*). The observed *B/A* ratios based on the refined Al(3A) and Al(3B) occupancies are 0.690 (6) (*H*) and 0.978 (8) (*S*). The (*H*) variety will thus only obey monoclinic symmetry, while the (*S*) variety is equally well described in orthorhombic symmetry as discussed above.

Structural comparison

The geometries of the fully occupied Si, Al(1A/B) and Al(2) sites are very similar for (*H*) and (*S*), and are also very similar to previously reported staurolite structures. The significant geometric differences are confined to the variably occupied Fe, U(A/B) and Al(3A/B) sites. A compilation of structural parameters of these sites from different refinements has been collected in Table 5. The largest differences are seen for the Al(3A/B) octahedra. The average Al(3A/B)—O distances are, as expected (Shannon, 1976), strongly correlated with the Al(3A/B) occupancy. Fig. 4 illustrates the correlation assuming $\frac{2}{3}\text{Al}$ and $\frac{1}{3}\text{Mg}$ in the Al(3A/B) sites. The data fall on two well separated straight lines. This difference is probably due to a difference in cation distributions. Extrapolating to $g = 0$ and $g = 1$ gives $\langle\text{Al}(3A/B)\text{—O}\rangle_{g=0} = 2.036$ and 2.034 \AA and $\langle\text{Al}(3A/B)\text{—O}\rangle_{g=1} = 1.930$ and 1.913 \AA for the upper and lower curves, respectively; $g = 0$ corresponds to an octahedron occupied by two hydrogens. The data from Tagai & Joswig (1985) (*d* in Fig. 4) contains an

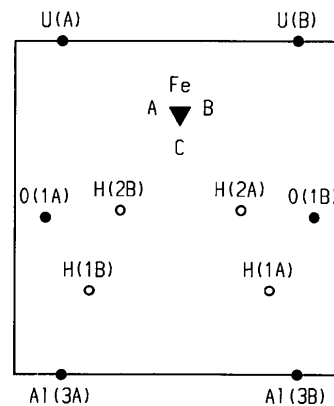


Fig. 3. Atomic sites in the $y = 0$ plane ($0 \leq x \leq 0.5$, $-0.1 \leq z \leq 0.6$). Hydrogen positions from Ståhl *et al.* (1988).

Table 5. Comparison of selected staurolite parameters

Occupancy factors, g , have been rescaled to correspond to pure Fe in the Fe and $U(A/B)$ sites and to $\frac{1}{3}\text{Al}$ and $\frac{1}{3}\text{Mg}$ in the $\text{Al}(3A/B)$ sites.

| | Heas | Scaer | SKS ^a | SM ^b | BG ^c | TJ ^d |
|---|-------|-------|------------------|-----------------|-----------------|-----------------|
| Radiation | X | X | N | X | X | N |
| T (K) | 293 | 293 | 13 | 293 | 293 | 100 |
| $g[\text{Al}(3A)]$ | 0.603 | 0.520 | 0.449 | 0.505 | 0.530 | 0.583 |
| $\langle \text{Al}(3A)-\text{O} \rangle$ (Å) | 1.972 | 1.981 | 1.979 | 1.973 | 1.979 | 1.982 |
| $g[\text{Al}(3B)]$ | 0.419 | 0.509 | 0.382 | 0.343 | 0.453 | 0.481 |
| $\langle \text{Al}(3B)-\text{O} \rangle$ (Å) | 1.992 | 1.982 | 1.988 | 1.992 | 1.987 | 1.984 |
| $g[U(A)]$ | 0.064 | 0.030 | 0.066 | 0.080 | 0.07 | 0.08 |
| $\langle U(A)-\text{O} \rangle$ (Å) | 2.165 | 2.164 | 2.159 | 2.165 | 2.154 | 2.162 |
| $g[U(B)]$ | 0.034 | 0.029 | 0.049 | 0.038 | 0.06 | 0.04 |
| $\langle U(B)-\text{O} \rangle$ (Å) | 2.162 | 2.164 | 2.158 | 2.163 | 2.153 | 2.162 |
| Q_{max} (Å ⁻¹) | 1.0 | 1.0 | 0.72 | 1.25 | 0.7 | 0.63 |
| $g(\text{Fe})$ | 0.818 | 0.857 | 0.732 | 0.834 | 0.767 | 0.76 |
| $\langle \text{Fe}-\text{O} \rangle$ (Å) | 2.006 | 2.005 | 2.000 | 2.008 | 1.998 | 2.004 |
| $B_{\text{iso}}(\text{Fe})$ (Å ²) | 1.25 | 1.22 | 1.01 | 1.01 | 1.19 | 1.01 |
| $\langle s_{\text{obs}} \rangle$ (Å) | 0.75 | 0.71 | 0.89 | 0.58 | 0.82 | ... |
| s_{calc} (Å) | 0.22 | 0.22 | 0.19 | 0.24* | 0.18 | 0.18 |

References: (a) Ståhl *et al.* (1988), (b) Smith (1968), (c) Bringham & Griffen (1986), (d) Tagai & Joswig (1985).

* From Fig. 5(b).

inconsistency in that the combined occupancy of the $\text{Al}(3A/B)$ and $\text{H}(1A/B)$ sites is well above unity.

The observed $\langle U(A/B)-\text{O} \rangle$ and $\langle \text{Fe}-\text{O} \rangle$ distances do not correlate obviously with the occupancy factors. The $U(A/B)$ occupancies are too low to give stable correlations and, as for the Fe site, substitutions with ions of different radii complicate a straightforward comparison. For instance, the shortest $\langle \text{Fe}-\text{O} \rangle$ and $\langle U(A/B)-\text{O} \rangle$ distances are found in the Co staurolite (Bringham & Griffen, 1986) since $r_{\text{Co}^{2+}} = 0.72$ and $r_{\text{Fe}^{2+}} = 0.77$ Å (Shannon, 1976). Variations in the H contents may also, through steric interactions, affect the $\langle \text{Fe}-\text{O} \rangle$ and, indirectly, the $\langle U(A/B)-\text{O} \rangle$ distances. Other important factors are the data-collection and refinement parameters. Calculations on the (H) data showed $\langle \text{Fe}-\text{O} \rangle$ to vary between 2.009 and 2.003 Å when the maximum $\sin\theta/\lambda$ varied between 0.5 and 1.0 Å⁻¹. Going from refinement mode (II) via model (I) to isotropic temperature factors decreases $\langle \text{Fe}-\text{O} \rangle$ from 2.006 to 2.0045 Å. The corresponding effects on other sites are much smaller. It is thus very difficult to draw any conclusions from variations below

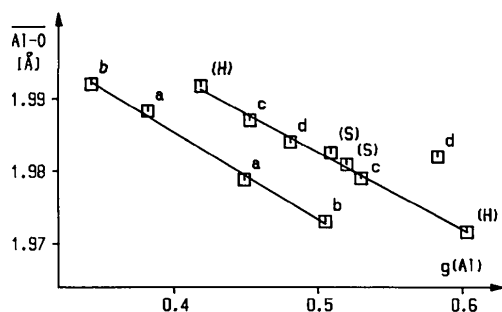


Fig. 4. $\langle \text{Al}(3A/B)-\text{O} \rangle$ versus $g[\text{Al}(3A/B)]$. Lettering for references according to Table 5.

0.005 Å unless equivalent data-collection and refinement parameters have been used.

Fe-site disorder

The temperature-factor coefficients of Fe are by far too large to represent only thermal motion. The isotropic mean value B_{iso} is found in the range 1.0–1.2 Å² in both X-ray and neutron diffraction experiments, independent of data-collection temperature. The expected B_{iso} from thermal motions of an ordered Fe site is of the order of 0.30 Å² and 0.7–0.9 Å² is apparently ascribable to disorder. A $\Delta\rho$ calculation by Smith (1968) revealed a threefold nature to the disorder, although the investigation used isotropic temperature factors and neglected anomalous-dispersion effects. A threefold splitting was also observed in a Co staurolite (Bringham & Griffen, 1986) and in the neutron study by Ståhl *et al.* (1988). The present study confirms the threefold nature of the disorder.

Qualitatively the threefold nature of the Fe disorder can be explained as a superposition of structural domains 1A, 1B, 3A and 3B. Close Fe—H contacts in domains 1A and 1B cause the two upper residual peaks in Fig. 1, while the absence of Fe—H repulsion in domains 3A and 3B causes the lower peak.

Quantitatively the site splitting can be estimated from the thermal parameters: a small unresolved site splitting will simply add to the refined thermal r.m.s. displacement. The excess in the thermal parameters caused by two-dimensional splitting may be obtained from the difference between temperature-factor coefficients parallel and perpendicular to the splitting. In the case of equilateral triangular splitting in the Fe site in staurolite the site separation is obtained from

$$(B_{33} - B_{22}) = s^2/3 \quad (1)$$

where the B_{ii} 's are elements of the mean-square displacement matrix and s the triangular side. The formula will increasingly underestimate s as s increases, and the calculated value of 0.22 Å for (H) and (S) was increased to 0.25 Å as a first estimate of the site separation.

Fe-site model calculations

In order to explore the effects of the Fe-site splitting, some model calculations were performed: a single anisotropic Fe site was refined against structure factors generated from a threefold-split isotropic Fe(A/B/C) site. Varying the Fe(A/B/C) parameters, the effects of site splitting, site occupancy and $\sin\theta/\lambda$ on an anisotropic Fe site were simulated. The results were compared in terms of the refined Fe position, the B_{iso} calculated from the refined anisotropic

temperature-factor coefficients and the separation and heights of the $\Delta\rho$ peaks. The results are summarized in Fig. 5. These calculations suggest the following:

(i) The separation of the $\Delta\rho$ peaks is not a simple function of the splitting of the model atoms (Fig. 5a). Below a certain site separation (0.25 Å), the peak separation is instead determined by the experimental resolution Q ($=\sin\theta/\lambda$) (Fig. 5c). The observed Q dependence largely explains the differences in previously reported peak separations ($\langle s_{\text{obs}} \rangle$ in Table 5).

(ii) The calculated B_{iso} is a simple function of the site splitting and is independent of the experimental resolution. Varying $B_{A/B/C}$ results in a corresponding variation in B_{iso} . Looking at the refined anisotropic temperature-factor coefficients they confirm a 10–20% underestimate of s by equation (1). Applying (1) with this correction to the Fe(A/B/C)-site splitting in previously reported staurolites, all fall in the range 0.20–0.25 Å.

(iii) The refined occupancy is, within 1% independent of site splitting, resolution and $B_{A/B/C}$.

(iv) Increasing the relative occupancy on one of the split positions results in a refined position closer to that site and *decreases* the corresponding $\Delta\rho$ peak height (Fig. 5d).

Fe-site refinements

A refinement model (III) based on an equilaterally split Fe site was then tried. The best fit was found with $s = 0.25$ Å. The remaining B_{iso} 's on the Fe(A/B/C) sites, 0.63 Å² (*H*) and 0.62 Å² (*S*), are still high compared with an ordered Fe site, but are reasonable considering that the model is restricted to equilateral-triangular splitting and does not allow for substitutional disorder. The ΔB_{iso} value, $B_{\text{iso}}[\text{model (I)}] - \langle B_{\text{iso}}[\text{Fe(A/B/C)}] \rangle$, of 0.6 Å² is consistent with the relationship found in Fig. 5(b). A test of the reliability of the refined $g(A/B/C)$ values was performed by calculating the occupancy-weighted-average Fe coordinates. The resulting coordinates, $\langle x \rangle$ and $\langle z \rangle$, are very close to those of refinement models (I) and (II) as seen in Table 2.

Cation-site assignment

The degrees of freedom in this system are too many to enable a unique cation assignment, and it is therefore necessarily based on a combination of the refined occupancies, chemical analyses and crystal-chemical reasoning. Some comments have to be given with the cation assignments. Generally, the analyses based on 48 O and 3 H correspond to a higher cation scattering power than observed in the structure refinements. The excess corresponds to less than two e.s.d.'s for (*H*) and less than one e.s.d. for (*S*) of the analyses, and is not alarming from a

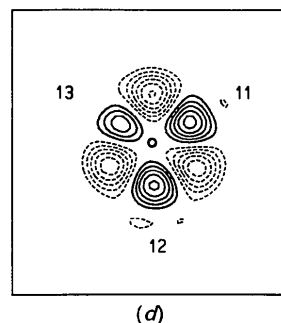
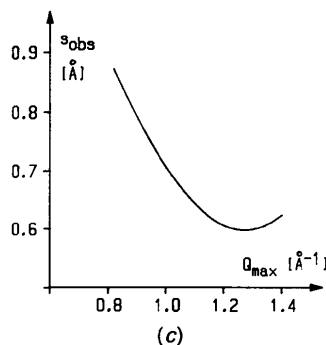
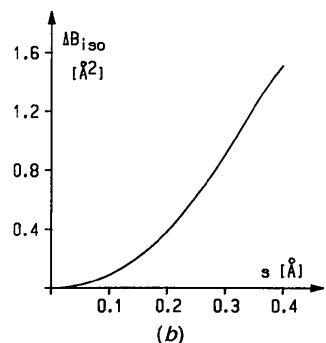
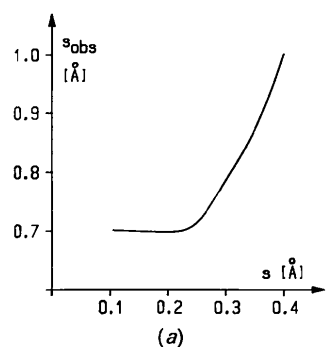


Fig. 5. Fe(A/B/C) site-model calculations. (a) Average distance between $\Delta\rho$ peaks versus model-atom splitting, $Q_{\text{max}} = 1.0 \text{ \AA}^{-1}$, $B_{A/B/C} = 0.40 \text{ \AA}^2$. (b) A plot of B_{iso} calculated from refined $B_{ij} - B_{A/B/C}$ versus model-atom splitting, $Q_{\text{max}} = 1.0 \text{ \AA}^{-1}$, $B_{A/B/C} = 0.40 \text{ \AA}^2$. (c) Average distance between $\Delta\rho$ peaks versus resolution, *i.e.* maximum $Q = \sin\theta/\lambda$ in calculations, $s = 0.25 \text{ \AA}$, $B_{A/B/C} = 0.40 \text{ \AA}^2$. (d) $\Delta\rho$ map for a case of unequal model-atom occupancy. Numbers denote relative occupancy.

statistical point of view. Including some Li [normally found at 0–0.4/48 O (Holdaway *et al.*, 1986)] will reduce the amounts of cations considered here in order to maintain charge balance. Assuming some Fe as Fe^{III} will have the same effect. Besides the problem of overall agreement there are many possibilities of interchanging cations between sites on the level of several percent.

The cation sites can be divided into two groups according to the refined occupancies: the Si, Al(1) and Al(2) sites show full occupancy while the Fe, *U* and Al(3) sites show a variable site occupancy. In the first group all Si is assigned to the Si site together with enough Al to give full occupancy. The reduced average charge of the Si site will lower the valence sum of O(4) and O(2) below two. This is compensated for in part by assigning the Ti contents, together with Al, to the Al(1) and Al(2) sites. Ti is, considering its ionic size, the most likely cation to substitute Al. In the second group more crystal-chemical assumptions have to be made. The Fe and *U* sites are assumed to be occupied by the same cations. The face-sharing of the tetrahedra about Fe with the octahedra about *U* suggests a close crystal-chemical relationship. The short Fe—*U* distances do not allow simultaneous occupancy of these sites and their combined occupancy may not exceed unity. The Fe occupancy has been shown to be further restricted by the presence of H(2) (Ståhl *et al.*, 1988). To fulfill the latter restriction it was necessary to assign almost all Fe to the Fe site. Also the Mn and Zn contents are assigned to the Fe and *U* sites together with enough Mg to match the refined occupancy in the (*S*) case. A corresponding amount of Mg was also added to the Fe and *U* sites in the (*H*) case. The remaining Al and Mg is then assigned to the Al(3) sites. The cation assignments are summarized in Table 6 and are essentially in agreement with model *b* in Ståhl *et al.* (1988).

The refined occupancies of the Fe(*A/B/C*) sites combined with their cation assignments can be used to obtain an estimate of the H contents. The H contents will be limited by the sum of occupancies of Fe(*A*) [H(1*A*)], Fe(*B*) [H(1*B*)] and the Fe-site vacancy [H(2*A/B*)] to 2.96 (*H*) and 2.66 (*S*). The values obtained here are in reasonable agreement with the assumed 3 H content, considering the possible errors in the cation assignments and the error limits assumed in the H analyses by Holdaway *et al.* (1986).

Concluding remarks

The presently studied staurolites agree with the domain description suggested by Ståhl *et al.* (1988). The Fe site is threefold disordered and its total occupancy is below unity (limited by neighbouring H sites) as predicted by the domain model. The Fe and

Table 6. Refined and calculated site populations (*p*) in staurolite from Heas and Scaer based on the scattering factors indicated by the site labels, and of Fe for the *U* sites

Numbers in parentheses represent e.s.d.'s from averaging of the four microprobe analyses of each crystal.

| | Refined <i>p</i> | Suggested site composition | Calculated <i>p</i> |
|--------------|---------------------|--|------------------------|
| Heas | | | |
| Si | 8 | 7.50 (3)Si 0.50Al | 7.96 |
| Al(1) | 8 | 15.91Al 0.09 (3)Ti | 8.03 |
| Al(2) | 8 | | |
| Fe | 3.269 (5) | 3.59 (6)Fe 0.10Mg 0.01 (1)Mn 0.01 (1)Zn | 3.46 |
| <i>U</i> | 0.196 (5) | 1.49Al 0.73Mg ΣAl = 17.90 (5) ΣMg = 0.83 (1) | 0.20 |
| Al(3) | 1.99 (1) | | |
| Scaer | | | |
| Si | 8 | 7.66 (7)Si 0.34Al | 7.98 |
| Al(1) | 8 | 15.89Al 0.11 (1)Ti | 8.04 |
| Al(2) | 8 | | |
| Fe | 3.427 (5) | 3.38 (2)Fe 0.23Mg 0.06 (2)Mn 0.04 (1)Zn | 3.46 |
| <i>U</i> | 0.119 (6) | 1.58Al 0.52Mg ΣAl = 17.81 (8) ΣMg = 0.75 (1) | 0.13 |
| Al(3) | 2.01 (1) | | |

U(*A/B*) sites are principally occupied by Fe²⁺ ions. The Fe(*A/B/C*) site separation is ~0.25 Å.

Model calculations indicate that neither the Δρ peak separation, nor the Δρ peak heights can be directly interpreted. The large variation in reported Δρ peak separations can instead be related to different experimental resolutions. The magnitude of the spatial disorder is more reliably estimated from the increase in the temperature-factor coefficients. It is thus suggested that the Fe(*A/B/C*) site separations in the presently and previously studied staurolite structures are all in the 0.20–0.25 Å range.

The strong correlation between bond lengths and occupancy factors for the Al(3*A/B*) sites at constant site composition indicates a far more restricted cation distribution at these sites than commonly assumed. The lack of such correlations for the Fe and *U*(*A/B*) sites suggests highly variable cation contents in these sites. In order to firmly establish the site distribution of various substituents it is suggested that future staurolite studies should include, for instance, EXAFS studies, or more elaborately, structural studies at wavelengths close to the absorption edges of the substituents using synchrotron radiation, on samples with large compositional variations.

Professor Jean Galy is gratefully acknowledged for providing facilities and for his constant interest in this work. We are also indebted to Drs Renee Enjalbert and Alain Mosset for supplying the single crystals for this investigation, and to Dr Francis Autefage for performing the microprobe analyses. KS thanks the Swedish Natural Science Research

Council and the French Centre National de la Recherche Scientifique for their financial support.

References

- ANDERSSON, S. & HYDE, B. G. (1982). *Z. Kristallogr.* **158**, 119–131.
- BECKER, P. J. & COPPENS, P. (1974). *Acta Cryst.* **A30**, 129–153.
- BRINGHURST, K. N. & GRIFFEN, D. T. (1986). *Am. Mineral.* **71**, 1466–1472.
- CHAURIS, L. & LE BAIL, F. (1968). *Penn Bed (Brest)*, **54**(6), 293–304.
- DOWTY, E. (1972). *Earth Planet. Sci. Lett.* **15**, 72–74.
- DUTROW, B. L., HOLDAWAY, M. J. & HINTON, R. W. (1986). *Contrib. Mineral. Petrol.* **94**, 496–506.
- GRIFFEN, D. T., GOSNEY, T. C. & PHILLIPS, W. R. (1982). *Am. Mineral.* **67**, 292–297.
- HANISCH, K. (1966). *Neues Jahrb. Mineral. Monatsh.* pp. 362–366.
- HOLDAWAY, M. J., DUTROW, B. L. & SHORE, P. (1986). *Am. Mineral.* **71**, 1142–1159.
- HOLLISTER, L. S. (1970). *Am. Mineral.* **55**, 742–766.
- HURST, V. J., DONNAY, J. D. H. & DONNAY, G. (1956). *Mineral. Mag.* **31**, 145–163.
- International Tables for X-ray Crystallography* (1974). Vol. IV. Birmingham: Kynoch Press. (Present distributor Kluwer Academic Publishers, Dordrecht.)
- LONKER, S. W. (1983). *Contrib. Mineral. Petrol.* **84**, 36–42.
- LUNDGREN, J.-O. (1983). *Crystallographic Computer Programs*. Report No. UUIC-B13-4-05. Univ. of Uppsala, Sweden.
- MOREAU, C. (1975). These 3^e Cycle, Univ. Paul Sabatier, Toulouse, France.
- NÁRAY-SZABÓ, I. (1929). *Z. Kristallogr.* **71**, 103–116.
- NÁRAY-SZABÓ, I. & SASVARI, K. (1958). *Acta Cryst.* **11**, 862–865.
- SCHWARZENBACH, D. (Chairman) *et al.* (1989). *Acta Cryst.* **A45**, 63–75.
- SHANNON, R. D. (1976). *Acta Cryst.* **A32**, 751–767.
- SMITH, J. V. (1968). *Am. Mineral.* **53**, 1139–1155.
- STÄHL, K., KVICK, Å. & SMITH, J. V. (1985). *Eos*, **66**, 400.
- STÄHL, K., KVICK, Å. & SMITH, J. V. (1988). *J. Solid State Chem.* **73**, 362–380.
- TAGAI, T. & JOSWIG, W. (1985). *Neues Jahrb. Mineral. Monatsh.* pp. 97–107.
- TAKÉUCHI, Y., AIKAWA, N. & YAMAMOTO, T. (1972). *Z. Kristallogr.* **136**, 1–22.

Acta Cryst. (1990). **B46**, 301–311

Lattice-Dynamical Estimation of Atomic Thermal Parameters for Silicates: Forsterite α - Mg_2SiO_4

BY TULLIO PILATI AND RICCARDO BIANCHI

CNR, Centro per lo Studio delle Relazioni tra Struttura e Reattività Chimica, Via Golgi 19, I-20133 Milano, Italy

AND CARLO MARIA GRAMACCIOLI

Dipartimento di Scienze della Terra, Università, Via Botticelli 23, I-20133 Milano, Italy

(Received 15 October 1989; accepted 20 December 1989)

Abstract

As an example of extending harmonic lattice-dynamical procedures to silicates, the atomic thermal parameters for forsterite Mg_2SiO_4 , an important constituent of earth's crust, have been calculated on this basis. For this purpose, Iishi's rigid-ion model [*Am. Mineral.* (1978), **63**, 1190–1197; 1198–1208] was used, with slight modifications. Although such potentials were derived exclusively from fitting IR and Raman-active frequencies, the reproduction of the phonon-dispersion curves is good, and the calculation of thermodynamic functions such as entropy provides values which are near to calorimetric estimates. The calculated atomic thermal parameters are in good agreement with the experimental values reported by most authors. The calculations at various temperatures show the effect of zero-point motion very clearly: its contribution to temperature factors is about half of the total at room temperature. Bond-length corrections for thermal libration

can be applied using the general-case formula: these amount to 0.003 Å for the Si—O bonds at room temperature. Although the thermal parameters in the SiO_4 group fit a rigid-body model, the correction obtained using the Schomaker–Trueblood procedure gives a significantly different result: this is essentially due to the weak librational character of the motion of silicate groups in the structure.

Introduction

The importance of atomic thermal parameters has been essentially discovered only recently; too often in fact they have been only considered as a substantial number of additional degrees of freedom to improve the final fit in least-squares refinements of crystal structures.

The first application of crystallographic thermal parameters to the problem of bond-distance correction was suggested by Cruickshank (1956) as a fit of